Society For Biomaterials

Modulation of Schlemm's canal endothelial cell stiffness via latrunculin loaded block copolymer micelles

Trevor Stack,[1] Amir Vahabikashi,[1] Mark Johnson,[1,2,3] Evan Scott [1,4,5,6,7]

[1]Department of Biomedical Engineering, Northwestern University, Evanston, 60208, Illinois
[2]Department of Mechanical Engineering, Northwestern University, Evanston, 60208, Illinois
[3]Department of Ophthalmology, Northwestern University, Chicago, 60611, Illinois
[4]Interdisciplinary Biological Sciences, Northwestern University, Evanston, 60208, Illinois
[5]Chemistry of Life Processes Institute, Northwestern University, Evanston, 60208, Illinois
[6]Simpson Querrey Institute, Northwestern University, Chicago, 60611, Illinois
[7]Robert H. Lurie Comprehensive Cancer Center, Northwestern University, Chicago, 60611, Illinois

Received 26 October 2017; revised 10 January 2018; accepted 14 February 2018
Published online 00 Month 2018 in Wiley Online Library (wileyonlinelibrary.com). DOI: 10.1002/jbm.a.36376

Abstract: Increased stiffness of Schlemm's canal endothelial cells (SC cells) is a major contributing factor to the increased pressure characteristic of primary open-angle glaucoma. New treatments for glaucoma are being developed using actin depolymerizers and rho kinase inhibitors to address this increased stiffness. However, these agents have off-target effects and are not as potent as had been hoped. We have developed a micellar nanocarrier assembled from poly(ethylene glycol)-*bl*-poly(propylene sulfide) copolymers capable of encapsulating latrunculin A (Lat A) with the goal of modulating SC cell stiffness. Lat A-loaded nanocarriers were similar in size and morphology to unloaded poly (ethylene glycol)-*bl*-poly(propylene sulfide) (PEG-*bl*-PPS) micelles, loaded Lat A at 62% encapsulation efficiency, and retained loaded Lat A for at least 22 days. The continued functional activity of Lat A following encapsulation within micelles was verified in murine macrophages, which are known to display decreased endocytosis in response to Lat A-dependent cytoskeletal disruption. Endocytic inhibition remained unchanged when comparing equal concentrations of micelle-loaded versus free form Lat A. Uptake of Lat A-loaded micelles by human SC cells was verified *in vitro* with no sign of cytotoxicity, and modulation of SC cell stiffness was measured by atomic force microscopy. Lat A-loaded micelles significantly decreased SC cell stiffness, which resulted in visible changes in cell morphology as observed by confocal microscopy. Our results demonstrate that PEG-*bl*-PPS micelles represent a tunable platform for the controlled intracellular delivery of latrunculin. These self-assembled polymeric nanobiomaterials may support the rational design and engineering of delivery systems for the treatment of glaucoma. © 2018 Wiley Periodicals, Inc. J Biomed Mater Res Part A: 00B:000–000, 2018.

Key Words: glaucoma, atomic force microscopy, self-assembly

How to cite this article: Stack T, Vahabikashi A, Johnson M, Scott E. 2018. Modulation of Schlemm's canal endothelial cell stiffness via latrunculin loaded block copolymer micelles. J Biomed Mater Res Part A 2015:00A:000–000.

INTRODUCTION

Glaucoma is a neurodegenerative disease often linked to abnormally high intraocular pressure and is the leading cause of irreversible blindness, affecting millions of people worldwide.[1] Intraocular pressure is primarily maintained by hydraulic resistance of the conventional outflow pathway, wherein aqueous humor exits the anterior chamber of the eye through the trabecular meshwork and Schlemm's canal (SC) endothelium. Glaucoma is associated with elevated stiffness of trabecular meshwork and SC inner wall endothelial cells, with the former possibly leading to the latter.[2] Increased stiffness of SC cells has been shown to impede pore formation within the SC endothelium, thereby increasing aqueous humor outflow resistance and elevating intraocular pressure.[3,4] Currently, most glaucoma therapies act by lowering aqueous inflow or increasing unconventional outflow, but these therapies do not address the fundamental pathology causing the elevated intraocular pressure.[5] New drug candidates targeting the conventional outflow pathway such as actin depolymerizers and rho

Correspondence to: E. Scott; e-mail: evan.scott@northwestern.edu
Contract grant sponsor: National Eye Institute; contract grant number: R01 EY01969
Contract grant sponsor: National Science Foundation CAREER Award; contract grant number: 1453576
Contract grant sponsor: National Institutes of Health Director's New Innovator Award; contract grant number: 1DP2HL132390-01
Contract grant sponsor: SPID facility at Northwestern University
Contract grant sponsor: Northwestern University – Flow Cytometry Core Facility (Cancer Center Support Grant); contract grant number: NCI CA060553

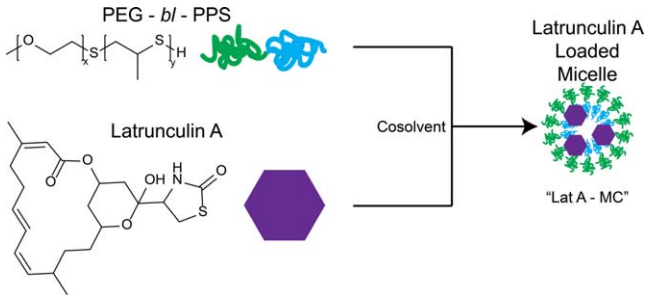

FIGURE 1. Graphical representation of the loading of micelles with Lat A.

kinase inhibitors are being developed[6] and will likely be additive in lowering intraocular pressure with existing treatments since they target distinct pathways for pressure reduction. However, actin depolymerizers and rho kinase inhibitors are associated with side effects such as corneal disorders[7] and conjunctival hyperemia.[8] Additionally, they have been shown to have less efficacy than desired at clinically relevant dosages. New and safer drugs targeting conventional outflow tissues are needed.

Latrunculin and other molecules that alter cell stiffness, such as rho kinase inhibitors, have been shown to change aqueous humor outflow resistance, thereby lowering the elevated intraocular pressure characteristic of glaucoma.[7] Latrunculin A (Lat A) is a well-characterized macrolide derived from sea sponge that induces actin depolymerization.[8] This transient depolymerization has many effects, including inhibition of endocytosis and decreased cell cytoskeletal integrity.[8,9] Lat A is frequently used to inhibit multiple forms of endocytosis by phagocytic cells, such as macrophages.[9] Both Lat A and its analog latrunculin B have been previously investigated in animal models and in clinical trials for the treatment of ocular hypertension in glaucoma.[10–14] A phase I clinical trial of latrunculin found only modest reduction in intraocular pressure at latrunculin concentrations that were more effective in primate eyes, and also found a high fraction of corneal disorders at the highest concentrations investigated.[15]

Nanobiomaterials have attracted much attention for their ability to deliver therapeutics and imaging agents to specific cells and tissues.[16,17] Increased specificity can improve efficacy and minimize off target effects to reduce cytotoxicity. Many drugs that had been previously seen to have insufficient efficacy or demonstrate cell cytotoxicity at therapeutic concentrations can be used with greater success when encapsulated in nanobiomaterials for selective uptake by relevant cell populations. In the case of glaucoma, SC cells have emerged as a potential therapeutic target,[4] and selective intracellular delivery of latrunculin to these cells through nanobiomaterials may increase efficacy at lower concentrations while avoiding uptake by neighboring cell types to decrease side effects. Nanobiomaterials self-assembled from poly (ethylene glycol)-*bl*-poly(propylene sulfide) (PEG-*bl*-PPS) copolymers have been employed as versatile nanocarriers for intracellular delivery both *in vivo* and *in vitro*.[18–22] Depending on their relative block lengths, they can be engineered to self-assemble into solid-core spherical micelles, vesicular polymersomes, or high aspect ratio filomicelles.[22–25] Self-assembly is driven by the hydrophobic PPS block, which also supports the loading and retention of a wide range of low water solubility therapeutics.[19,21] PEG-*bl*-PPS nanocarriers are also highly stable under physiological conditions due to a very low critical micelle concentration of approximately $10^{-7}M$.[24] These nanobiomaterials possess a dense PEG corona that provides a neutral, hydrophilic surface to resist protein adsorption, reduce nonspecific cell interactions and support custom chemical modification for specific applications. We have found nanocarriers and hydrogels composed of PEG-*bl*-PPS to be nonimmunogenic and exceptionally noninflammatory following both bolus and sustained delivery.[17,22] PEG functionalized nanobiomaterials also allow for versatile surface modification with targeting moieties such as peptide sequences, allowing for enhanced targeting of desired cell populations.

Encapsulation in PEG-*bl*-PPS micelles presents a method for targeted intracellular delivery of latrunculin to SC cells, while reducing off target effects. As a first step in the rational design of targeted nanocarriers capable of treating glaucoma, we demonstrate here a nanobiomaterial formulation for the intracellular delivery of latrunculin (Fig. 1) and subsequent modulation of SC cell stiffness. Loading efficiency and stability of Lat A was characterized, and preservation of its functional effects following intracellular delivery through PEG-*bl*-PPS micelles was verified using a macrophage endocytic inhibition assay. Morphological effects of Lat A-loaded micelles on SC cells was directly observable by fluorescence microscopy, and changes in cell stiffness was quantified by atomic force microscopy (AFM).

MATERIALS AND METHODS

Synthesis of PEG-*bl*-PPS copolymer

Nanocarriers were fabricated based on the controlled self-assembly of PEG-*bl*-PPS block copolymers. A variety of different morphologies can be obtained by controlling the molecular weight (MW) ratio of the hydrophilic PEG to hydrophobic PPS blocks. PEG_{45}-*bl*-PPS_{26} block copolymers were synthesized as previously described.[19,22] Briefly, PEG thioacetate was deprotected by sodium methoxide for initiation of anionic ring opening polymerization of propylene sulfide. The reaction was run to completion and

subsequently protonated with acetic acid to create the PPS thiol-end groups for subsequent fluorophore conjugation. The resulting block copolymer was purified by double precipitation in methanol and then characterized by 1H NMR ($CDCl_3$) and gel permeation chromatography (ThermoFisher Scientific) using Waters Styragel columns with refractive index and ultraviolet−vis detectors in a tetrahydrofuran mobile phase.

Assembly and loading of PEG-*bl*-PPS micelles

Micelles were assembled from PEG-*bl*-PPS polymer using the cosolvent evaporation method as described previously.[23] PEG_{45}-*bl*-PPS_{26} block copolymer and 10 μg LAT A (Cayman Chemical) were dissolved in 0.5 mL dichloromethane (DCM). Copolymer and Lat A solutions in DCM were added dropwise to a sterile scintillation vial containing 1 mL of vigorously stirred phosphate buffered saline (PBS). DCM was allowed to evaporate for 4 h. Maleimide functionalized Alexa Fluor 555 (Thermo Fisher) was then added (0.024 m*M*:10 mg polymer) to PBS while being stirred and allowed to react for 4 h. Resulting micelles were purified by gravity column chromatography using a Sephadex LH 20 column (Sigma-Aldrich) in PBS. Recovered micelles were further purified and concentrated using 7000 MW cutoff Zebaspin desalting columns (Thermo Fisher).

Characterization of PEG-*bl*-PPS micelles

The size distribution and zeta potential of the nanostructures were analyzed by Zetasizer Nano (Malvern Instruments) with a 4 mW He−Ne 633 nm laser at 1 mg/mL in PBS. The polydispersity index (PDI) was calculated using a two-parameter fit to the dynamic light scattering (DLS) correlation data. The morphology of assembled micelles was determined by cryogenic transmission electron microscopy (Gatan) (cryoTEM) as previously described.[18] In order to determine Lat A encapsulation efficiency, 100 μL of purified micelles were frozen at −80°C and subsequently lyophilized overnight. Lat A was extracted from the resulting cake using methanol. After 4 h of extraction, the suspension was centrifuged for 5 min at 4000*g* and supernatant was evaluated for Lat A concentration using high performance liquid chromatography (HPLC). A 95:5 methanol:water mobile phase was used on an Agilent C18 XDB-Eclipse column. Absorption at 235 nm was used to measure the Lat A concentration. Standard curves were generated by serial dilution of Lat A, followed by the same freeze, lyophilize, and extract procedure described above.

Cell culture

Normal SC cells (SC78) were a generous gift from the laboratory of Dr. Stamer at Duke University. The protocol for SC cell extraction from postmortem human eyes is described in detail elsewhere.[26] Extracted cells were shipped overnight to our lab in T-25 flasks filled with dulbecco's modified eagle's medium (DMEM)/low glucose (Life Technologies) with 10% fetal bovine serum (FBS) (Atlanta Biologicals) and 1% penicillin/streptomycin (Life Technologies). Upon arrival, the culture media was replaced with fresh media and flasks were stored in the incubator at 37°C and 5% CO_2. Cells were trypsinized and passaged at 1:3 ratio when 80% confluent. We used SC cells at passage 5 for both AFM and imaging experiments.

RAW264.7 macrophages were purchased from ATCC and shipped frozen on dry ice. Upon arrival, cells were cultured in T75 polystyrene tissue culture treated flasks (BD Falcon) with DMEM (Life Technologies), 10% FBS (Gibco), and 1% penicillin/streptomycin (Life Technologies). Once 75%–80% confluent, cells were passaged through mechanical cell scraping.

Flow cytometry to assess cell viability

Cell viability assays were performed using Zombie Aqua fixable cell viability dye. Cells were plated at 10,000–20,000 cells/cm^2 in 48 well tissue culture treated plates and allowed to adhere and proliferate for overnight. Adherent cells were washed with PBS and treatments of 0.5, 1, 2, and 4 μ*M* Lat A micelles (as determined by loaded Lat A quantity) and free Lat A were administered for 4 h. Additionally, control groups treated with PBS and TritonX-100 were included. At the end of the incubation, media was harvested, and SC cells were removed from the plate through trypsinization. To determine cell viability, cells were stained with Zombie Aqua fixable viability dye (Biolegend) for 15 min, then washed with PBS and fixed with intracellular (IC) cell fixation buffer (Biosciences). Flow cytometry data was obtained using FACSdiva software on a LSRII flow cytometer (BD Biosciences) and the resulting data was analyzed using cytobank software.

Flow cytometry to quantify nanocarrier uptake by cells

SC cells or RAW264.7 macrophages adhered to tissue culture treated 48 well polystyrene plates (Falcon), were treated with Alexa fluor 555 conjugated micelles described above for 4 h. After incubation, cells were washed with PBS and harvested using trypsin or cell scraping method. Cells were stained with Zombie Aqua fixable viability dye, and then washed and fixed with IC cell fixation buffer (Biosciences). Flow cytometry was performed with FACSdiva on a LSRII flow cytometer (BD Biosciences), with the phycoerythrin (PE) channel being used to detect nanocarrier uptake. Data was analyzed using Cytobank software (Cytobank).

Dextran pHrodo chase assay

RAW264.7 Macrophages were cultured in DMEM (Life Technologies) + 10% FBS (Life Technologies) +1% penstrep (Life Technologies) media in 12 well tissue culture treated polystyrene plates (BD Falcon) until 75% confluent at which point treatments ($n = 3$) were applied (controls, 0.1, 0.5, and 1 μ*M* Lat A micelles, 1 μ*M* Free Lat A). Treatments were incubated with cells at 37°C for 2 h, and subsequently 15 μg/mL pHrodo red dextran dye (Thermo Fisher) was added to each well for 15 min. After this incubation, cells were washed with PBS and cell staining buffer and removed from 12 well plates by cell scraping method. Control groups included PBS treatment with no pHrodo chase, PBS treatment with a pHrodo chase, and cells treated with 1 μM Lat A micelles with no pHrodo chase. These groups were used to normalize flow data. Data were normalized as a percentile of uptake inhibition between the

maximum uptake (pHrodo chase) and minimum uptake (PBS treatment).

Atomic force microscopy

SC cells were seeded in 60 mm petri-dishes (VWR, Batavia, IL) 48 h prior to the experiment and were confluent at the time of measurement. A BioScope II with NanoscopeV controller (Bruker, Santa Barbara, CA) coupled to an inverted fluorescent microscope with ×10 (NA = 0.3), ×20 (NA = 0.8) objective lens was used to make AFM measurements (Carl Zeiss, Thornwood, NY). We used spherical polystyrene probes with nominal diameter of 10 μm (Novascan Technologies, Ames, IA) mounted on a silicon nitride cantilever with nominal spring constant of 0.01 N/m. The cantilever spring constant was calibrated before the experiment using Thermal Tune module of the Nanoscope. During the AFM experiments, cells were maintained in culture medium and a heated stage maintained a constant temperature of 37°C. The indentation depth was limited to 400 nm to avoid substrate effects and the tip velocity was adjusted to 800 nm/s to avoid viscous effects. The force measurements were done at regions well away from cell nucleus and periphery to avoid the nucleus and substrate effect, respectively. Each cell was probed only once and at least 15 measurements were made for each sample group. Data from AFM measurements were used to extract force versus indentation curves and the Hertz model was then utilized to calculate the Young's modulus of the cells as described previously.[27]

Laser scanning confocal microscopy of SC cells

Four glass coverslips (22 × 22 No. 1.5, Thermo Fischer Scientific, MA) were sterilized (dipped in 70% ethanol and flamed on a Bunsen burner) and placed inside the wells of a six-well culture dish (Thermo Fischer Scientific, MA). SC cells were seeded into the four wells of the culture dish 48 h prior to the treatment. The culture media was DMEM/low glucose (Life Technologies, Grand Island, NY) with 10% fetal bovine serum (Atlanta Biologicals, Norcross, GA) and 1% penicillin/streptomycin (Life Technologies, Grand Island, NY). On the day of the experiment, fresh culture media was used to create the treatment cocktails for the four experimental groups. The first treatment group was SC cells with plain culture media; the second was SC cells incubated with unloaded micelles; the third was the SC cells incubated with 0.5 μ*M* Lat A solution; and the fourth group was the SC cells incubated with the Lat A-loaded micelles at a latrunculin concentration of 0.5 μ*M*. Lat A of 0.5 μ*M* was chosen based on previous studies by our own group and others.[4,7,12] All groups were incubated with their corresponding cocktails for 2 h. Coverslips were then gently washed with PBS and fixed with 4% paraformaldehyde (Electron Microscopy Sciences, Hatfield, PA) for 10 min at room temperature. Fixed cells were gently rinsed with PBS twice, permeabilized with 0.2% Triton (Life Technologies, Grand Island, NY) for 5 min then rinsed again with PBS twice. Samples were next stained for F-actin (30 min incubation with one volume per test of Alexa Fluor® 568 Phalloidin, (Life Technologies, Grand Island, NY) and cell nucleus (10 min incubation with Hoechst 33342 (1:10,000), Thermo Fischer Scientific, Grand Island, MA) and rinsed with PBS twice. Stained slides were mounted on microscope glass slides (Thermo Fischer Scientific, Grand Island, NY) using 6 μL of fluorescence mounting medium (Dako, Carpinteria, CA) and cured in the dark at 4°C for 24 h. Afterward, the slide edge was covered with nail polish (Electron Microscopy Sciences, Hatfield, PA) and cured at dark at 4°C for one day. A Zeiss 510 LSM inverted confocal microscope was used to create optical sections and confocal images of the samples.

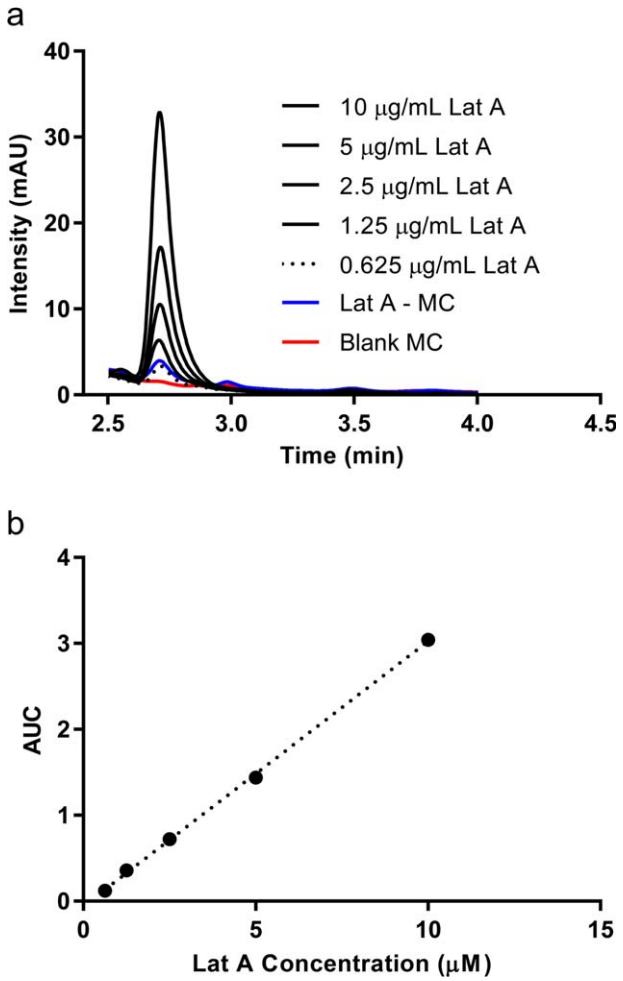

FIGURE 2. Loading of Lat A into PEG-*bl*-PPS micelles. Following assembly and loading through nanoprecipitation, Lat A concentrations within micelles were quantified using (a) HPLC that referenced a reproducible (b) standard curve of serially diluted free form Lat A. A 95:5 methanol:water mobile phase and Lat A were detected by absorption at 235 nm. All reported concentrations of Lat A and loaded micelles (Lat A-MC) refer to Lat A concentrations determined by this HPLC-based method. One example measurement (blue line) of micelle loading quantification is shown, which matched the concentration of free form Lat A at 0.625 mg/mL (dotted line).

RESULTS

Loading of Lat A into PEG-*bl*-PPS micelles can be quantified by HPLC and does not influence micelle structure

To investigate the structure of PEG_{45}-*bl*-PPS_{26} micelles encapsulating Lat A, loaded and unloaded micelles were

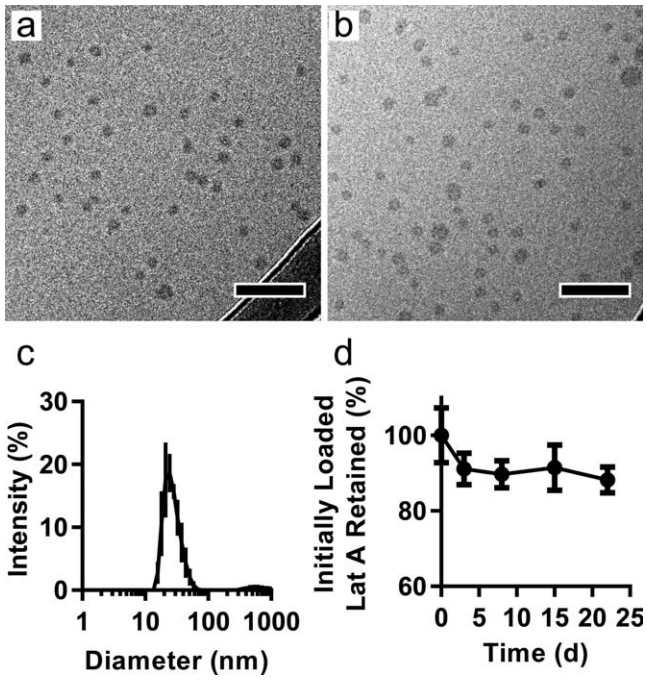

FIGURE 3. PEG-*bl*-PPS nanocarrier characterization. Representative cryoTEM image of (a) blank micelles and (b) Lat A-loaded micelles. Scale bar: 100 nm. (c) Size determination of Lat A-loaded micelles by DLS; (d) Stability of Lat A loading within micelles over a 22 day period. Micelles were incubated at room temperature inside a 1000 MW cutoff dialysis filter and dialyzed against PBS. Lat A micelles were sampled at various time points and analyzed by HPLC using a methanol extraction method. Three separate batches were analyzed, data presented as mean ± SD ($n = 3$ experimental replicates).

produced from the same self-assembling block copolymer through cosolvent evaporation. Quantification of Lat A loading was achieved using HPLC that allowed all formulations tested to be referenced in terms of the overall Lat A concentration in the solution, whether in free or micelle-loaded form (Fig. 2). The resulting materials were imaged using cryoTEM to identify the micelle morphology and representative size (Fig. 3). The micelles were further characterized by DLS (Table I). There were no significant differences in either morphology or size between loaded and unloaded micelles demonstrating that loading of Lat A did not significantly impact PEG-*bl*-PPS self-assembly.

Lat A is consistently and stably loaded into PEG-*bl*-PPS micelles

We next quantified the encapsulation and stability of Lat A in PEG-*bl*-PPS micelles using HPLC. Loaded Lat A was isolated from micelles by disrupting micellular structure through lyophilization and subsequent extraction of Lat A in methanol. Loading efficiency was found to have a consistent range from 55% to 65% across multiple rounds of micelle formation, which falls near our expected range of loading based on the partition coefficient of Lat A (logP: 3.86).[18,28] To evaluate the stability of this loading over time, Lat A-loaded micelles were dialyzed against PBS and sampled at various time points out to 22 days after initial formation. The quantity of Lat A was found to decrease to 90% of the initially loaded amount and then remained stable at that value through 22 days after initial loading [Fig. 3(d)]. We expect Lat A to be retained in our PEG-*bl*-PPS polymer due to the highly stable nature of the self-assembled structure as well as the relative hydrophobicity of Lat A.

Lat A-loaded micelles reduce macrophage endocytosis in a dose dependent manner

Intracellular Lat A is known to depolymerize actin filaments in cells to inhibit several forms of endocytosis and is routinely employed in assays to investigate mechanisms of nanobiomaterials endocytosis by phagocytic cells.[29] As observed previously for PEG-*bl*-PPS nanocarriers,[19] macrophages readily endocytosed Lat A micelles in a dose dependent manner [Fig. 4(a)]. To verify that Lat A remains functional when loaded within PEG-*bl*-PPS micelles, we evaluated their functional ability to reduce uptake by RAW macrophages using a pulse chase experiment with fluorescent dextran. RAW264.7 cells were treated with three separate

TABLE I. Size, Polydispersity, and Loading Efficiency for Lat A-Loaded PEG-*bl*-PPS Micelles

Sample	Z-avg (nm)	PDI	Loading	Mass Drug/Mass Polymer
Blank micelles	30.74 ± 0.57	0.11	N/A	N/A
Lat A-micelles	26.07 ± 0.38	0.15	62.3%	10 μg/20 mg

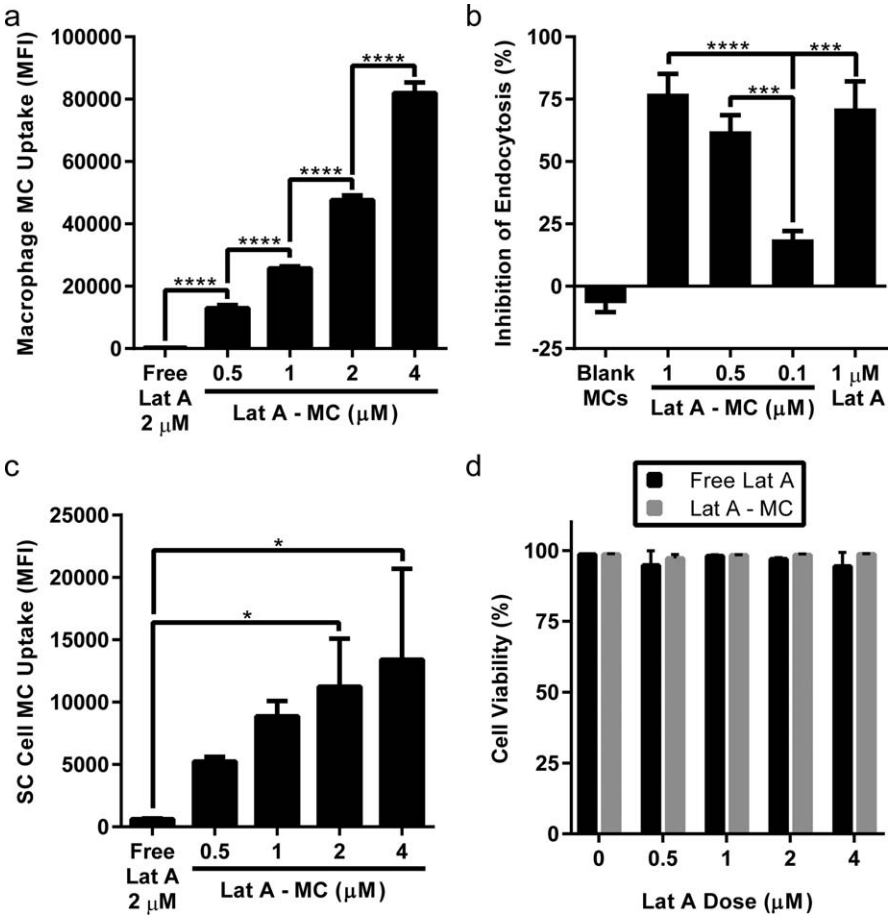

FIGURE 4. Flow cytometry verified that Lat A-loaded micelles are endocytosed by RAW macrophages and SC cells with no observable cytotoxicity. Single cell mean fluorescence intensity (MFI) of Alexa fluor 555 conjugated micelles was measured to quantify uptake by RAW Macrophages (a) and SC cells (c) after 4 h of treatment. Continued bioactivity of Lat A loaded within micelles was verified using a pulse chase assay (b). Following a 2 h incubation with different concentrations of Lat A micelles, inhibition of the uptake of a dextran pHrodo chase dye by RAW264.7 macrophages was compared to a free form 1 μM Lat A control. Cell viability of SC cells following incubation with Lat A-loaded micelles was assessed by staining with Zombie Aqua fixable viability dye and subsequent fixation (d). Lat A micelle values shown are for dose of loaded Lat A administered. Data shown as mean ± SD ($n = 3$ biologic replicates). p values shown as follows: ****$p < 0.0001$, ***$0.0001 < p < 0.001$, **$0.001 < p < 0.01$, *$0.01 < p < 0.05$.

doses of Lat A-loaded micelles or free Lat A, washed and then incubated with a dextran conjugated pHrodo dye chase. Dextran can enter macrophages through receptor mediated endocytosis, macropinocytosis and micropinocytosis.[30,31] These dyes are pH sensitive and increase their fluorescence intensity with increasing acidity, meaning that they should increase in intensity as they move through the endocytic pathway into the lysosome. We found that the inhibition of dextran uptake, increased with increasing Lat A micelle dose [Fig. 4(b)]. We also found that equivalent doses (1 μM Lat A) of free Lat A and Lat A micelles did not produce significantly different amounts of dextran uptake, indicating that function between the two groups is quite similar.

Lat A micelles are endocytosed by SC cells and are not cytotoxic

We sought to ensure that PEG-*bl*-PPS micelles were endocytosed by SC cells, and also that there was no resulting cytotoxicity. SC cells were treated with free Lat A in free (0.5–4 μM) and micelle loaded (0.5–4 μM) form for 4 h, then harvested and evaluated for micelle uptake and cytotoxicity through flow cytometry. Flow cytometric analysis revealed the amount of fluorescence per cell increased with micelle dosage, and there was less fluorescence observed in SC cells than macrophages [Fig. 4(a, c)]. This is most likely due to the highly phagocytic nature of RAW macrophages compared to SC cells. SC cells showed no significant decreases in cell viability due to either free Lat A or Lat A-loaded micelles, indicating no cytotoxicity regardless of delivery vehicle up to 4 μM dosages [Fig. 4(d)]. These results demonstrate that PEG-*bl*-PPS micelles can achieve intracellular delivery of Lat A without inducing cellular toxicity.

Lat A-loaded micelles modulate the morphology and stiffness of SC cells

To evaluate the effects of Lat A micelles on SC cells, we assessed changes in cell morphology and stiffness. SC cells were treated with 0.5 μM Lat A micelles for between 30 min and 4 h, and subsequently evaluated through confocal microscopy and AFM. Following treatment with Lat A

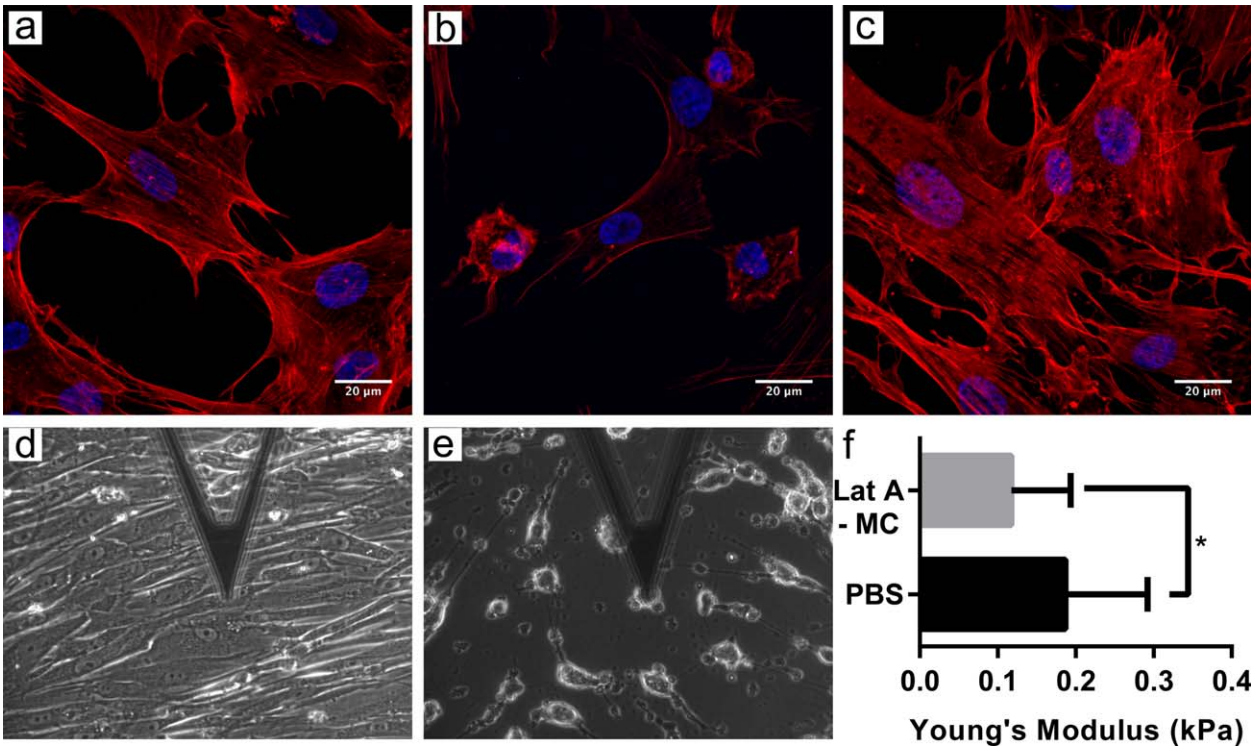

FIGURE 5. Representative images of SC cells treated with PBS (a, d), Lat A-loaded micelles (0.5 μ*M* of Lat A; 0.91 mg PEG-*bl*-PPS) (b, e) and blank PEG-*bl*-PPS micelles (0.91 mg PEG-*bl*-PPS) (c). Confocal images (a–c), were stained with phalloidin actin stain (red) and Hoescht 33342 (blue). AFM phase contrast images were taken during stiffness measurements (d, e). Stiffness of SC cells after treatment for 2 h was determined by AFM (f). Data are shown as geometric mean ± SD about geometric mean and analyzed using an unpaired t-test, $*0.01 < p < 0.05$.

micelles, confocal images revealed rounding up of the SC cells, while no morphological changes were seen when the cells were treated with blank micelles (Fig. 5). Furthermore, AFM revealed a significantly decreased stiffness of nearly 50% for SC cells when treated with Lat A micelles (Fig. 5). These results demonstrate both a qualitative and quantitative functional effect of the Lat A micelles on SC cells.

DISCUSSION

Here, we have demonstrated PEG-*bl*-PPS nanocarrier encapsulation and intracellular delivery of Lat A, a potent inhibitor of actin polymerization, for modulation of SC cells. Glaucomatous SC cells have been identified as having increased stiffness as compared to SC cells from normal eyes, and this increased stiffness is thought to cause increased aqueous humor outflow resistance and thereby may contribute to the elevated pressure characteristic of glaucoma.[4] Latrunculin has been proposed as a possible treatment for glaucoma[13,14,32] but has not moved forward to clinical use. We hypothesize that a nanobiomaterial formulation of Lat A will be able to reduce off target effects while increasing efficacy through enhanced intracellular delivery. As a first step to engineer such a targeted delivery system, we loaded Lat A into PEG-*bl*-PPS micelles and assessed their functional activity on macrophages and SC cells. We first characterized the loaded micelles themselves using a variety of techniques (Figs. 2 and 3). Lat A was consistently and stably loaded into PEG-*bl*-PPS micelles, while maintaining structural characteristics similar to unloaded micelles. As such, we would expect these micelles to have biodistributions similar to our previously reported data on intravenous injections of PEG-*bl*-PPS micelles.[22] These data also support our previous findings that hydrophobic drugs can be loaded into PEG-*bl*-PPS micelles at therapeutically relevant concentrations without negatively impacting the assembled nanocarrier stability and morphology.[18,21,22,33]

To assess any changes or decreases in Lat A function as a result of encapsulation by PEG-*bl*-PPS micelles, we evaluated the ability of Lat A in either free or micelle loaded form to inhibit endocytosis of fluorescent dextran by RAW264.7 macrophages using a pulse chase experiment. This murine cell line is easily obtainable and one of the most frequently utilized phagocyte models to assess cellular interactions with nanobiomaterials.[21,34–36] Lat A micelles were found to be functionally equivalent at the same latrunculin solution concentrations as free form Lat A. In the case of molecules active in the cytosol, such as Lat A, synthetic self-assembled block copolymers like PEG-*bl*-PPS provide mechanisms for endosomal escape,[19,21] potentially enhancing the ability for Lat A to interact with the actin cytoskeleton. Furthermore, cells have unique surface interactions with nanoscale biomaterials that can exploit diverse mechanisms of cell entry that are not available to small molecules, particularly by promoting receptor clustering required for several mechanisms of receptor mediated endocytosis.[37–40] Thus, enhancement of both endocytosis and intracellular

delivery may allow micelles to achieve efficacy despite their larger size and resulting slower diffusion rates in solution when compared to solubilized small molecules.

Having established that Lat A remained functional when delivered through micelles using a standard model of macrophage endocytosis, we assessed their ability to modulate the more therapeutically relevant and difficult to obtain human SC cells. Nanocarrier uptake by SC cells visibly changed the morphology of SC cells and significantly decreased cell stiffness. Retention assays were verified by HPLC and showed that over the course of at least 24 h, Lat A was not leaking out of nanocarriers at functionally relevant levels. This indicated that PEG-*bl*-PPS micelles achieved intracellular delivery of Lat A and that these payloads reached sufficient cytosolic concentrations to modulate the SC cell cytoskeleton. We have previously demonstrated this effect of latrunculin on SC cells,[41] but here we demonstrate that a micellar delivery system, which could decrease nonspecific cellular interactions during *in vivo* application, can deliver functionally active Lat A to the SC cell interior. The previously demonstrated versatility of PEG-*bl*-PPS copolymer chemistry and control over self-assembly will allow further development of these nanobiomaterials for enhanced selectivity of Lat A delivery and avoidance of unwanted side effects during *in vivo* applications, such as through surface conjugation of SC cell-specific targeting moieties and optimization of nanocarrier structure.[17,18,21,22,33] PEG-*bl*-PPS nanocarriers therefore present a stable platform for intracellular delivery of Lat A to SC cells that is amenable to further modification for optimization of *in vivo* applications, potentially resulting in a more efficacious and patient friendly glaucoma treatment.

ACKNOWLEDGMENTS

We thank Dr. W Daniel Stamer of Duke University for the gift of SC cells. The authors acknowledge Jonathan Remis (Structural Biology Facility, NU) for his contribution to cryoTEM sample prep and image acquisition.

REFERENCES

1. Quigley HA, Broman AT. The number of people with glaucoma worldwide in 2010 and 2020. Br J Ophthalmol 2006;90:262–267.
2. Russell P, Johnson M. Elastic modulus determination of normal and glaucomatous human trabecular meshwork. Invest Ophthalmol Vis Sci 2012;53:117.
3. Zhou EH, Krishnan R, Stamer WD, Perkumas KM, Rajendran K, Nabhan JF, Lu Q, Fredberg JJ, Johnson M. Mechanical responsiveness of the endothelial cell of Schlemm's canal: scope, variability and its potential role in controlling aqueous humour outflow. J R Soc Interface 2012;9:1144–1155.
4. Overby DR, Zhou EH, Vargas-Pinto R, Pedrigi RM, Fuchshofer R, Braakman ST, Gupta R, Perkumas KM, Sherwood JM, Vahabikashi A, Dang Q, Kim JH, Ethier CR, Stamer WD, Fredberg JJ, Johnson M. Altered mechanobiology of Schlemm's canal endothelial cells in glaucoma. Proc Natl Acad Sci 2014;111:13876–13881.
5. Kopczynski CC, Epstein DL. Emerging trabecular outflow drugs. J Ocul Pharmacol Ther 2014;30:85–87.
6. Karmel M. Glaucoma pipeline drugs: Targeting the trabecular meshwork. Am Acad Ophthalmol 2013;10:38–43.
7. Andrés-Guerrero V, García-Feijoo J, Konstas AG. Targeting Schlemm's canal in the medical therapy of glaucoma: Current and future considerations. Adv Ther 2017;34:1049–1069.
8. Spector I, Shochet NR, Blasberger D, Kashman Y. Latrunculins–novel marine macrolides that disrupt microfilament organization and affect cell growth: I. Comparison with cytochalasin D. Cell Motil Cytoskeleton 1989; 13: 127–144.
9. Dutta D, Donaldson JG. Search for inhibitors of endocytosis. Cellular Logistics 2012; 2: 203–208.
10. Okka M, Tian B, Kaufman PL. Effects of latrunculin b on outflow facility, intraocular pressure, corneal thickness, and miotic and accommodative responses to pilocarpine in monkeys. Trans Am Ophthalmol Soc 2004;102:251–260.
11. Thomasy SM, Wood JA, Kass PH, Murphy CJ, Russell P. Substratum stiffness and latrunculin B regulate matrix gene and protein expression in human trabecular meshwork cells. Invest Ophthalmol Vis Sci 2012;53:952–958.
12. Rasmussen CA, Kaufman PL, Ritch R, Haque R, Brazzell RK, Vittitow JL. Latrunculin B reduces intraocular pressure in human ocular hypertension and primary open-angle glaucoma. Transl Vis Sci Technol 2014;3:1.
13. Peterson JA, Tian B, Bershadsky AD, Volberg T, Gangnon RE, Spector I, Geiger B, Kaufman PL. Latrunculin-A increases outflow facility in the monkey. Invest Ophthalmol Vis Sci 1999;40:931–941.
14. Peterson JA, Tian B, Geiger B, Kaufman PL. Effect of Latrunculin-B on outflow facility in monkeys. Exp Eye Res 2000;70:307–313.
15. Rasmussen CA, Kaufman PL, Ritch R, Haque R, Brazzell RK, Vittitow JL. Latrunculin B reduces intraocular pressure in human ocular hypertension and primary open-angle glaucoma. Transl Vis Sci Technol 2014;3:1.
16. Allen S, Liu YG, Scott E. Engineering nanomaterials to address cell-mediated inflammation in atherosclerosis. Regen Eng Transl Med 2016;2:37–50.
17. Scott EA, Karabin NB, Augsornworawat P. Overcoming immune dysregulation with immunoengineered nanobiomaterials. Annu Rev Biomed Eng 2017;19:57–84.
18. Allen S, Osorio O, Liu Y-G, Scott E. Facile assembly and loading of theranostic polymersomes via multi-impingement flash nanoprecipitation. J Control Release 2017;262:91–103.
19. Scott EA, Stano A, Gillard M, Maio-Liu AC, Swartz MA, Hubbell JA. Dendritic cell activation and T cell priming with adjuvant- and antigen-loaded oxidation-sensitive polymersomes. Biomaterials 2012;33:6211–6219.
20. Stano A, Scott EA, Dane KY, Swartz MA, Hubbell JA. Tunable T cell immunity towards a protein antigen using polymersomes vs. solid-core nanoparticles. Biomaterials 2013;34:4339–4346.
21. Vasdekis AE, Scott EA, O'Neil CP, Psaltis D, Hubbell JA. Precision intracellular delivery based on optofluidic polymersome rupture. ACS Nano 2012;6:7850–7857.
22. Yi S, Allen SD, Liu Y-G, Ouyang BZ, Li X, Augsornworawat P, Thorp EB, Scott EA. Tailoring nanostructure morphology for enhanced targeting of dendritic cells in atherosclerosis. ACS Nano 2016;10:11290–11303.
23. Cerritelli S, O'Neil CP, Velluto D, Fontana A, Adrian M, Dubochet J, Hubbell JA. Aggregation behavior of poly(ethylene glycol-*bl*-propylene sulfide) di- and triblock copolymers in aqueous solution. Langmuir 2009;25:11328–11335.
24. Napoli A, Tirelli N, Wehrli E, Hubbell JA. Lyotropic behavior in water of amphiphilic ABA triblock copolymers based on poly(propylene sulfide) and poly(ethylene glycol). Langmuir 2002;18:8324–8329.
25. Segura T, Hubbell JA. Synthesis and in vitro characterization of an ABC triblock copolymer for siRNA delivery. Bioconjug Chem 2007;18:736–745.
26. Stamer WD, Roberts BC, Howell DN, Epstein DL. Isolation, culture, and characterization of endothelial cells from Schlemm's canal. Invest Ophthalmol Vis Sci 1998;39:1804–1812.
27. Vargas-Pinto R, Gong H, Vahabikashi A, Johnson M. The effect of the endothelial cell cortex on atomic force microscopy measurements. Biophys J 2013;105:300–309.
28. Sterling T, Irwin JJ. ZINC 15–Ligand discovery for everyone. J Chem Inf Model 2015;55:2324–2337.
29. Iversen TG, Skotland T, Sandvig K. Endocytosis and intracellular transport of nanoparticles: Present knowledge and need for future studies. Nano Today 2011;6:176–185.

30. Araki N, Johnson MT, Swanson JA. A role for phosphoinositide 3-kinase in the completion of macropinocytosis and phagocytosis by macrophages. J Cell Biol 1996;135:1249–1260.
31. Norbury CC. Drinking a lot is good for dendritic cells. Immunology 2006;117:443–451.
32. Peterson JA, Tian B, McLaren JW, Hubbard WC, Geiger B, Kaufman PL. Latrunculins' effects on intraocular pressure, aqueous humor flow, and corneal endothelium. Invest Ophthalmol Vis Sci 2000;41:1749–1758.
33. Dowling DJ, Scott EA, Scheid A, Bergelson I, Joshi S, Pietrasanta C, Brightman S, Sanchez-Schmitz G, Van Haren SD, Ninković J, Kats D, Guiducci C, de Titta A, Bonner DK, Hirosue S, Swartz MA, Hubbell JA, Levy O. Toll-like receptor 8 agonist nanoparticles mimic immunomodulating effects of the live BCG vaccine and enhance neonatal innate and adaptive immune responses. J Allergy Clin Immunol 2017;140:1339.
34. Oh N, Park JH. Endocytosis and exocytosis of nanoparticles in mammalian cells. Int J Nanomed 2014;9 Suppl 1:51–63.
35. Anselmo AC, Zhang M, Kumar S, Vogus DR, Menegatti S, Helgeson ME, Mitragotri S. Elasticity of nanoparticles influences their blood circulation, phagocytosis, endocytosis, and targeting. ACS Nano 2015;9:3169–3177.
36. Herd H, Daum N, Jones AT, Huwer H, Ghandehari H, Lehr C-M. Nanoparticle geometry and surface orientation influence mode of cellular uptake. ACS Nano 2013;7:1961–1973.
37. Rossman JS, Leser GP, Lamb RA. Filamentous influenza virus enters cells via macropinocytosis. J Virol 2012;86:10950–10960.
38. Gao H, Shi W, Freund LB. Mechanics of receptor-mediated endocytosis. Proc Natl Acad Sci USA 2005;102:9469–9474.
39. Nel AE, Mädler L, Velegol D, Xia T, Hoek EMV, Somasundaran P, Klaessig F, Castranova V, Thompson M. Understanding biophysicochemical interactions at the nano-bio interface. Nat Mater 2009;8:543–557.
40. Zhang J, Xia F, Yang Y, Yue C, Zhang C, Yang Y, Ma L, Alfranca G, Liu Y, Hou Y, Jin W, Ni J, Fuente JMdl, Cui D. Human CIK cells loaded with gold nanoprisms as theranostic platform for targeted photoacoustic imaging and enhanced immuno-photothermal combined therapy. Nanotechnol Biomed Eng 2016;8:112–127.
41. Zhou EH, Krishnan R, Stamer WD, Perkumas KM, Rajendran K, Nabhan JF, Lu Q, Fredberg JJ, Johnson M. Mechanical responsiveness of the endothelial cell of Schlemm's canal: scope, variability and its potential role in controlling aqueous humour outflow. J R Soc Interface 2012;9:1144–1155.